Electric Potential Estimation of Inhomogeneous and Differentially Charged Objects Using X-Rays

Julian Hammerl *, Andrea López † and Hanspeter Schaub ‡
University of Colorado Boulder, Boulder, Colorado 80303

A sensing method has been proposed that aims at estimating discrete electric potentials of nearby objects in space remotely using x-rays. Terrestrial experiments with a complex-shaped and differentially charged test object were conducted in recent work, and a new approach based on theoretical x-ray models was proposed that enables the simultaneous measurement of two different potentials from a single recorded x-ray spectrum. However, the test object consisted of only two differentially charged components made of the same material. The theoretical x-ray model used for the simultaneous measurement of multiple potentials depends on the material of the target object, so inhomogeneity of the object considerable affects the proposed method. This paper experimentally investigates the remote electric potential estimation of objects with multiple differentially-charged components made of different materials using x-rays.

I. Introduction

Spacecraft naturally charge in the plasma environment in orbit due to ambient electrons and ions impacting the spacecraft, and due to photons from the Sun exciting electrons that leave the craft. Some of the consequences of spacecraft charging affect the individual satellite. If the spacecraft is not fully conducting, some components build up different electric potentials than others, called differential charging. Even though spacecraft design guidelines recommend to connect all satellite components to one common ground [1], old satellites or spacecraft that have been exposed to the space environment for a considerable time might not be fully conducting. This can lead to arcing between parts and potentially damage the spacecraft or reduce the lifetime of the solar panels [2, 3].

Other consequences of spacecraft charging are inter-craft effects between two nearby satellites. Arcing can occur between two satellites during docking if the two spacecraft are charged to significantly different electric potentials. Different potentials on two nearby satellites are especially likely if one spacecraft eclipses the other, as this blocks the sunlight that is responsible for the photoelectric current from reaching the eclipsed spacecraft while the sunlit spacecraft is subject to this current. By estimating the electric potential of each spacecraft prior to docking, one can decide whether it is safe to dock or the risk of electrostatic discharge too high. High electric potentials of spacecraft also result in electrostatic forces between two nearby craft. Spacecraft can naturally charge to several kilovolts in geostationary orbit, resulting in forces in the order of milli-Newtons. Additionally, these forces lead to electrostatic torques if the center of charge of each craft does not align with the center of mass. The forces and torques can significantly perturb the relative motion during proximity operations [4]. If one craft is uncooperative, for example during on-orbit servicing operations, the electrostatic torque will cause it to tumble, and the servicing satellite needs to match the rotational rate to maintain a constant relative orientation. This can lead to increased fuel consumption of the servicing mission. One way to mitigate the effect of such electrostatic perturbations is to estimate the electric potential of the target object and use this information to predict the resulting forces. The predicted forces and torques are then fed-forward to the relative motion controller [5] to reduce control effort and minimize the rotational rates of the target.

It is also of interest to actively charge spacecraft to high potentials and utilize the resulting forces. The Electrostatic Tractor, for example, is an active debris removal method that takes advantage of inter-craft electrostatic forces [6]. Using an electron gun that is attached to the servicing satellite and aimed at a retired satellite in geostationary orbit, the servicer charges positively to tens of kilovolts due to the emission of electrons while the debris charges negatively due to the accumulation of electrons. These high electric potentials result in a significant attractive force between the two craft that acts like a virtual tether and is used to tug the retired satellite to a graveyard orbit. The Electrostatic Tractor

*Graduate Research Assistant, Ann and H.J. Smead Department of Aerospace Engineering Sciences, AIAA Student Member. julian.hammerl@colorado.edu

†Graduate Research Assistant, Ann and H.J. Smead Department of Aerospace Engineering Sciences, AIAA Student Member.

‡Professor and Department Chair, Schaden Leadership Chair, Ann and H.J. Smead Department of Aerospace Engineering Sciences, AIAA Fellow.

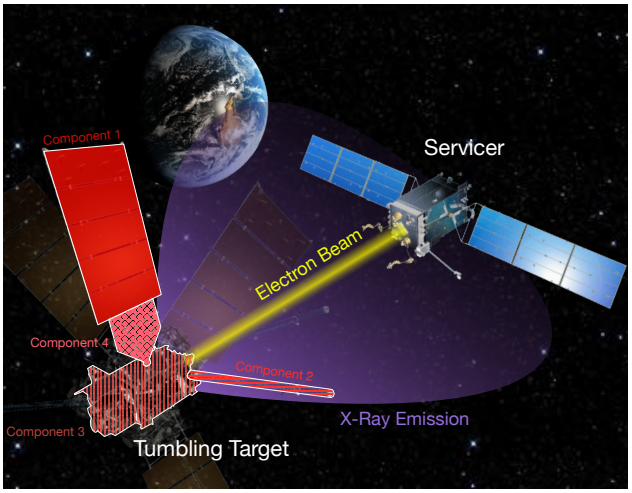

Fig. 1 Concept of touchlessly sensing the electric potential of an inhomogeneous and differentially charged object using the x-ray method

benefits from remote electric potential estimation in two ways. First, to maintain a constant desired potential on both spacecraft, active charge control is needed to adjust the electron beam current as the two-craft formation travels through the changing plasma environment in geostationary orbit. Such charge control requires feedback of the electric potential of the servicer and the debris. Second, the relative motion control of the Electrostatic Tractor feeds forward the expected electrostatic force between the two satellites to improve the control performance [7]. Remote estimation of the debris electric potential is necessary to obtain a good prediction of the electrostatic forces.

Two methods to remotely sense electric potentials of nearby objects in space have been recently proposed: the electron method [8] and the x-ray method [9]. Both methods utilize an electron gun on a servicing satellite that is aimed at the object of interest. As the electrons from the electron beam impact on the target object, secondary electrons and x-rays are excited. The secondary electrons are released with negligible kinetic energy and, if the potential of the target object is negative, are accelerated away from the target object. The increase in kinetic energy of those electrons that are on trajectories toward the servicer corresponds to the difference in electric potentials between the target object and the servicer. Thus, if the potential of the servicer is known, the electric potential of the target is inferred by measuring the kinetic energy of the secondary electrons at the servicing satellite. This is referred to as the electron method. The x-ray method takes advantage of the interaction of the beam emitted by the electron gun with the electric field generated by the charged spacecraft. The initial kinetic energy of the electron beam is known and corresponds to the operating energy of the electron gun. As the electron beam electrons travel from the servicing satellite toward the target object, they are either accelerated or decelerated, depending on whether the electric potential difference between the two craft is positive or negative, respectively. The gain or loss in kinetic energy of the electron beam is equal to the electric potential difference, so by measuring the kinetic energy when the beam impacts the target, one can infer the potential of the target if the potential of the servicer is known. It is assumed that the target object is uncooperative, so no instrument to measure the energy of the electrons is available. Instead, the x-ray spectrum of the excited x-rays is used. X-rays are emitted with an energy up to the landing energy of the incoming electrons. By finding the maximum photon energy in the recorded spectrum, the landing energy is estimated and the electric potential of the target object inferred. The electric potential of a neighboring object in space can also be passively determined by looking at the x-rays that are generated by the ambient plasma environment, without using an active electron beam on the servicing craft [10].

Prior research on the x-ray method discussed the theory of remotely sensing electric potential using x-ray spectroscopy [9]. An x-ray spectrum consists of two different types of radiation. Characteristic radiation is emitted at a discrete energy that is specific for each element and allows for material identification. Bremsstrahlung radiation is emitted at continuous energies up to the landing energy of the incoming electrons. Terrestrial experiments in the Electrostatic Charging Laboratory for Interactions between Plasma and Spacecraft (ECLIPS) research vacuum chamber [11] showed that it is possible to estimate electric potentials with errors of less than 100 V using this method [12]. The experiments were performed using flat plate target objects at various orientations. More recent work used spacecraft shape primitive test objects consisting of two components, a cube acting as the spacecraft bus and a panel [13]. Both components

were made of aluminum, but charged to different potentials. This allows to study the effects of complex shapes and differential charging on the x-ray method. The electric field due to the charged object and consequently the trajectory of the electron beam depend on the electric potential of the components and the orientation of the target object. The results of the experiments show that, for given electric potentials of the components, the landing location of the electron beam is determined by the orientation of the object. Because the potential of a component can only be measured if x-rays are excited from that component, the orientation of the target object influences what potential is measured. If the target object is static and the electron beam only impacts on one component, only one potential can be measured at a time. Reference 13 also proposed a new approach to measure multiple potentials simultaneously with one recorded x-ray spectrum by using the principle of superposition and theoretical x-ray models. This approach was tested in Ref. [14] using a rotating target object that causes the electron beam to impact on different components during the x-ray recording time frame, resulting in a recorded x-ray spectrum that includes information about the potential of two components charged to different potentials. The results show that it is possible to measure two potentials of a rotating target object simultaneously with a single recorded x-ray spectrum.

All prior experiments were conducted with components made of the same material. The theoretical x-ray models that are used to measure multiple potentials simultaneously depend on the material composition of the x-ray source, so the presence of components made of different materials complicates the proposed approach. In this work, experiments are conducted with inhomogeneous target objects with more than two components made of different materials and charged to different potentials.

II. Theory of Potential Estimation using X-rays and Experimental Setup

A. X-ray Spectroscopic Potential Estimation

Two different types of x-ray radiation are generated when energetic electrons impact on an object. The first type, called characteristic x-ray radiation, occurs when an incoming electron removes an inner-shell electron. This causes an outer-shell electron of the atom to fill the empty spot, and a characteristic photon with an energy equal to the energy difference between the two shells is released [15, Chapter 10]. The difference in energy between the shells is specific for each element, so characteristic x-ray radiation can be used for material identification. The second type of x-ray radiation is referred to as Bremsstrahlung, German for breaking radiation: when an electron passes closely by an atomic nucleus, it is decelerated, and the loss in energy is emitted as an x-ray photon [15, Chapter 10]. Because this interaction can occur in many different ways, the amount of kinetic energy lost in the process can be any value up to the initial energy of the electron as it impacts on the surface material (referred to as landing energy or effective energy). If the electron is fully stopped during its interaction with a single nucleus, the energy of the emitted photon is equal to the landing energy of the electron, given by the Duane-Hunt law [16]. Thus, while characteristic x-ray radiation provides a way to identify the material of an object, the Bremsstrahlung radiation allows for the determination of the landing energy of the impacting electrons.

An electron gun mounted on a servicing spacecraft is proposed to be used to excite the x-rays from a target object [9]. As the electrons travel from the servicer to the target, the kinetic energy of the electrons changes due to the electric field generated by the two charged spacecraft. If the potential of the target is lower (more negative or less positive) than that of the servicer, the electrons are decelerated. If the potential of the target spacecraft is higher (less negative or more positive), the electrons are accelerated as they are attracted towards the target. The difference in kinetic energy between the initial location of the electrons (at the servicer) and at the final location (at the target) is equal to the difference in electric potential between the two spacecraft. The initial energy of the electrons is known as it corresponds to the operating energy of the electron gun, and the electric potential of the servicer can be measured using a Langmuir probe [17]. Thus, by determining the landing energy of the electrons from a recorded x-ray spectrum, the electric potential of the target can be estimated [9, 12]. This method makes no assumption regarding the polarity of the potential of either spacecraft, and can be used to estimate both negative and positive potentials of the target. Note that the electron beam induces a current to the target object which affects the potential of the target. This effect is considered out-of-scope for this work. In the experiments, high voltage power supplies are used to maintain a nearly constant electric potential on the target object.

Due to the noise in the recorded x-ray spectrum, it is not sufficient to simply take the highest photon energy observed in the spectrum. Instead, a more robust approach is implemented that takes advantage of the nearly linear shape of the Bremsstrahlung spectrum close to the landing energy [18]. A linear curve is fitted to the upper energy part of the spectrum. The energy at which this line intersects the x-axis is taken as the estimation of the landing energy [12]. This

spectroscopic approach does not require any knowledge about the material of the object, the estimation is based solely on the recorded spectrum.

B. Theoretical X-ray Spectrum

While the spectroscopic method explained above only uses the recorded spectrum to estimate the electric potential, the approach introduced in Ref. 19 to measure multiple potentials simultaneously requires the computation of a theoretical x-ray spectrum. The theoretical models employed in this work are based on thick targets. Such models assume that the incident electron is fully stopped in the target. Given that electrons are typically stopped within a few micro-meters for the electron beam energies used in this work (up to 12 keV), this assumption is valid for the 0.85 mm panels and the cube [19]. The theoretical models are described in greater detail in Ref. 19, but summarized here for convenience.

The number of characteristic x-ray photons due to K_α transitions excited per incident electron with energy E_e is approximated by [20]

$$I_{ph,c}(E_e) = \begin{cases} N\left(\frac{E_e}{E_k} - 1\right)^\alpha & \text{if } E_e \geq E_k \\ 0 & \text{if } E_e < E_k \end{cases} \tag{1}$$

where the parameters N, α and the characteristic energy E_k are material dependent. Because the characteristic energy E_k is the energy of the emitted characteristic photons, the energy of the incoming electron E_e must be greater than E_k to excite characteristic photons. The x-ray detector senses a Gaussian distribution with a width defined by the full width at half maximum (FWHM). For the detector used in this work, the FWHM is approximately 140 eV and is converted to the standard deviation of the Gaussian distribution by

$$\sigma = \frac{\text{FWHM}}{2\sqrt{2\ln(2)}} \tag{2}$$

Given the standard deviation and the number of characteristic photons per incident electron with energy E_e, the theoretical characteristic radiation as observed by the detector is computed using the normal distribution

$$I_{ph,c,\text{det}}(E, E_e) = \frac{I_{ph,c}(E_e)}{\sigma\sqrt{2\pi}} \exp\left(-\frac{(E - E_k)^2}{2\sigma^2}\right) \tag{3}$$

The integral of this Gaussian distribution is $I_{ph,c}(E_e)$, so the number of photons per incident electron are redistributed from a discrete energy E_k to a Gaussian distribution with standard deviation σ.

The number of Bremsstrahlung x-ray photons with energy between E_e and $E_e + \Delta E$ (with bin size ΔE) excited per incident electron with energy E_e is estimated by [21]

$$\begin{aligned} I_{ph,b}(E, E_e) = C\sqrt{Z}\frac{E_e - E}{E}\left(-73.90 - 1.2446E + 36.502\ln(Z) + \frac{148.5E_e^{0.1293}}{Z}\right)\cdot \\ \cdot\left(1 + (-0.006624 + 0.0002906E_e)\frac{Z}{E}\right)\Delta E \end{aligned} \tag{4}$$

with atomic number Z and using a scaling factor C. The total number of photons N_{ph} with an energy of E that are sensed by the detector during an accumulation time of Δt is computed by

$$N_{ph}(E, E_e) = \frac{I_{EB}}{q}\Omega\Big[I_{ph,c,\text{det}}(E, E_e) + I_{ph,b}(E, E_e)\Big]\Delta t \tag{5}$$

where I_{EB} is the electron beam current and $q$is the elementary charge. The solid angle Ω is determined by $\Omega = \frac{A_{\text{det}}}{L^2}$, with the detector area A_{det} and the distance of the detector from the x-ray source L. The efficiency of the x-ray detector is also considered [*]. The parameters N, E_k, α, Z and C are shown in Tab. 1 for aluminum, copper and titanium. For titanium, the data from Ref. 22 is used to determine the scaling factor C.

[*]https://www.amptek.com/products/x-ray-detectors/sipin-x-ray-detectors/sipin-x-ray-detectors (Consulted on: 11/25/2022)

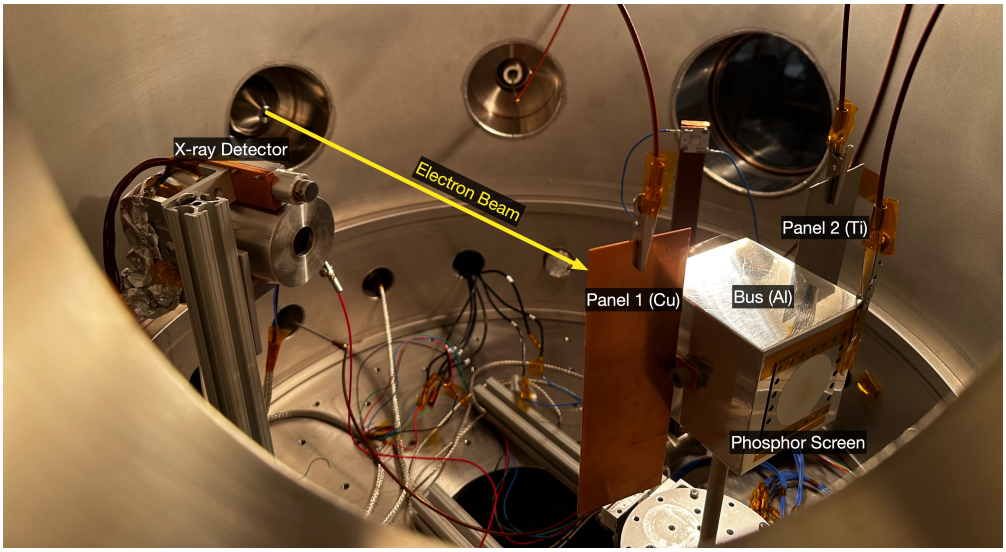

Fig. 2 Experimental setup with a box-and-panel object representing a spacecraft

C. Experimental Setup

All experiments are performed in the ECLIPS spacecraft charging research vacuum chamber [23]. The primary components of the experimental setup, shown in Fig. 2, include an electron gun, an x-ray detector, and a target object consisting of a bus and two panels. The spacecraft bus is a $70 \times 70 \times 70$ mm aluminum (Al) cube, one panel is made of copper (Cu) and the other panel is made of titanium (Ti). The dimension of both panels is $155 \times 50 \times 0.85$ mm. Non-conducting Polyetheretherketone (PEEK) screws and washers are used to connect the panels with the cube to electrically isolate the components from each other. The target object is on top of an RM-3 vacuum compatible rotary platform from Newmark Systems that makes it possible to change the orientation of the target. A PEEK rod is used to connect the cube with the rotary stage. The orientation of the cube is measured with an incremental rotary high-vacuum Renishaw Tonic encoder.

An EMG-4212C electron gun from Kimball Physics is used, which is capable of emitting electrons with energies from 1-30 keV and currents from 1 µA to 100 µA. The focus of the beam is adjustable, and the beam steering option of the electron gun allows to control the direction of the beam to some extent. This is convenient because the landing location of the beam can be moved from one target component to another without rotating the target object. An Amptek X123 X-ray detector with a 6 mm^2 Si-PIN diode is used to record the x-ray spectrum, and the line between the x-ray detector and the test object approximately forms a 16° angle with the electron beam. A Rugged Phosphor Screen from Kimball Physics with a diameter of 3.8 cm is mounted on one side of the cube to visually verify the landing location of the electron beam on thee cube when all components are grounded. The angle that describes the orientation of the target object is defined to be zero when the phosphor screen is facing the electron beam (perpendicular to the unperturbed, straight electron beam). Finally, the potential of the three components (i.e. cube, copper panel and titanium panel) is controlled by three high voltage power supplies (HVPS). Two Matsusada AU-30R1 power supplies are used to control the potential of the cube and the titanium panel, and are capable of providing potentials up to 30 kV. The potential of the copper panel is maintained by a Spellman SL300 power supply that is limited to potentials of up to 1 kV.

Table 1 Theoretical x-ray model parameters

Element	N	E_k	α	Z	C
Aluminum (Al) [20]	1.4×10^{-5}	1.49 keV	1.63	16	3.35×10^{-7}
Copper (Cu) [20]	6.4×10^{-5}	8.05 keV	1.63	29	9.78×10^{-7}
Titanium (Ti) [20, 22]	2.2×10^{-5}	4.50 keV	1.55	22	3.20×10^{-7}

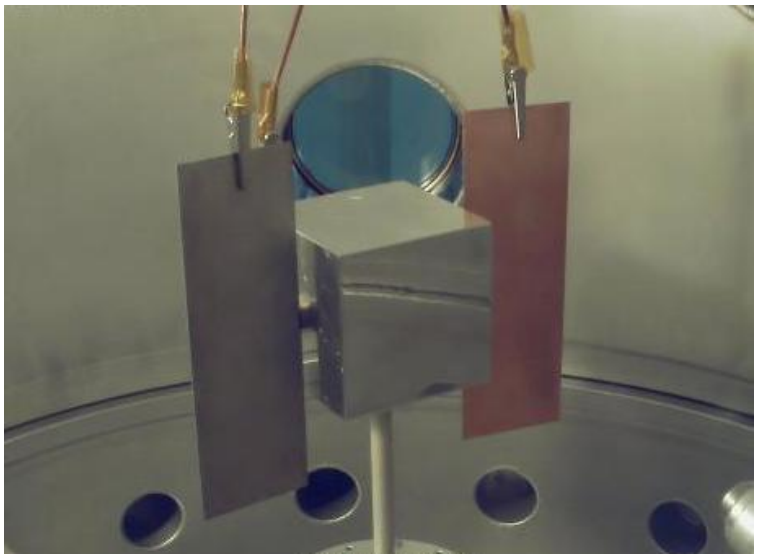

Fig. 3 Target object at an angle of 210 **degrees. View from above the electron gun.**

III. Results

A. Beam Steering

The electron gun of the ECLIPS facility has the capability to steer the electron beam in the X and Y direction (perpendicular to the direction of the beam) by applying a voltage between −300 V and +300 V to two separate deflection grids located near the exit of the electron gun. By changing the deflection voltages, one can aim the electron beam at different locations and components without changing the orientation of the target. This capability is employed here to excite x-rays separately from each of the three target components and the chamber wall. An electron beam energy of $E_{EB} = 12$ keV is used with a beam current of $I_{EB} = 5$ µA. The beam focus is set to $V_F = 6$ V, resulting in a spot size of about 3 mm in diameter, and the orientation of the target is set to an angle of 210 degrees. Various deflections in the X direction between −300 V and +300 are used, and 10 spectra are recorded for each deflection, over a time period of 20 seconds. All components of the target are at different potentials, with the bus at $V_B = -5$ kV, panel 1 (Cu) at $V_{P1} = -1$ kV, and panel 2 (Ti) at $V_{P2} = -3$ kV. The resulting spectra for all 10 runs per deflection are shown in Fig. 4 for four different beam deflections. The mean over all 10 spectra per deflection is indicated by the black curve, and the fitted linear curves that are used to estimate the potential are plotted in blue. For a deflection voltage of $V_X = -300$ V, the beam is deflected off to the right of the target and hits the grounded chamber wall, resulting in characteristic peaks at 5.4 keV and 6.4 keV, corresponding to Chromium (Cr) and Iron (Fe), respectively. Decreasing the magnitude of deflection to $V_X = -90$ V causes the beam to hit the copper panel, exciting characteristic x-rays for Copper (Cu) with energies of 8.0 keV and 8.9 keV. For a straight beam ($V_X = 0$ V), the x-rays are excited from the cube, resulting in characteristic photons with an energy of 1.5 keV that correspond to Aluminum (Al). Finally, if the beam is deflected as much as possible to the left ($V_X = 300$ V), the beam impacts on the Titanium (Ti) panel with a corresponding characteristic peak in the recorded spectrum at 4.5 keV. All characteristic energy values are taken from the X-ray Transition Energies Database provided by the National Institute of Standards and Technology (NIST) [24]. Note that the signal-to-noise ratio in the higher energy part of the spectra is relatively low, requiring the approach with the fitted linear curve to estimate the potential.

Figure 5 shows a box plot with the estimated potential for each value of deflection. The horizontal line inside of each box corresponds to the median of the data, and the bottom and top edges of the box represent the 25% and 75% percentiles. The black whiskers indicate the minimum and maximum of each data set, excluding outliers. Outliers are represented by circles and are values that are more than $1.5 \cdot IQR$ away from the bottom or top of the box, where IQR is the difference between the top and bottom box edges (interquartile range). The estimated potentials are reasonable accurate, with the exception of the titanium panel. One possible reason for this could be the relatively weak x-ray signal from the titanium panel, as the panel is located on the far side of the cube with respect to the x-ray detector, and part of the cube is blocking the sensor's view of the panel.

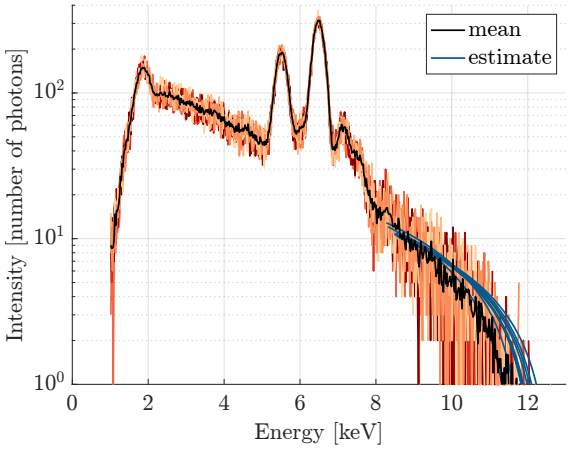

(a) Steel chamber wall (0 kV): X-Deflection $V_X = -300$ V

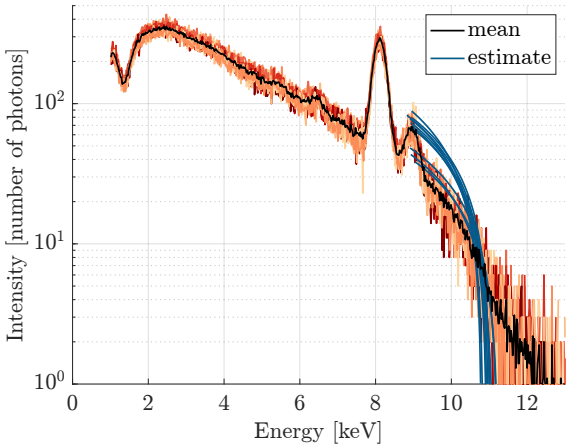

(b) Copper panel (-1 kV): X-Deflection $V_X = -90$ V

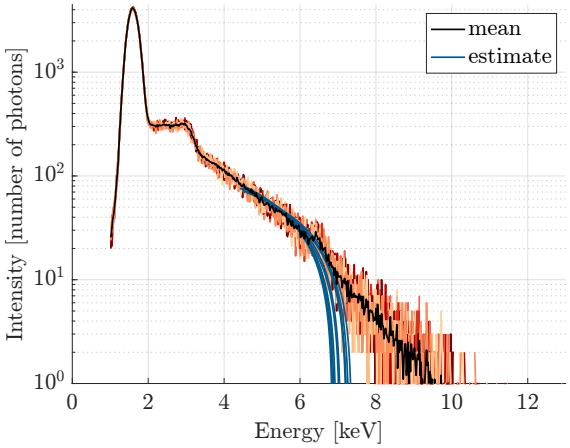

(c) Aluminum bus (-5 kV): X-Deflection $V_X = 0$ V

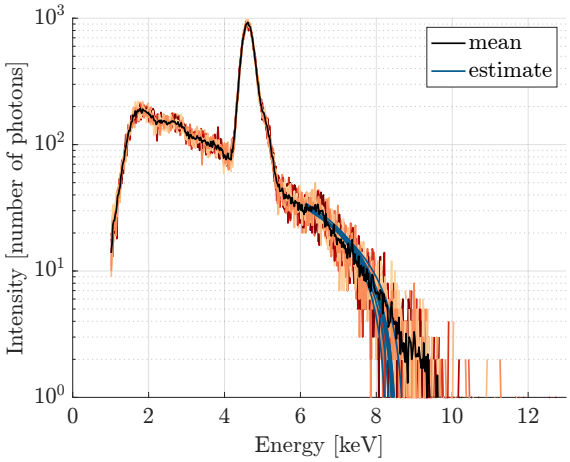

(d) Titanium panel (-3 kV): X-Deflection $V_X = 300$ V

Fig. 4 Individual x-ray spectra for different beam deflections. 10 recorded spectra each

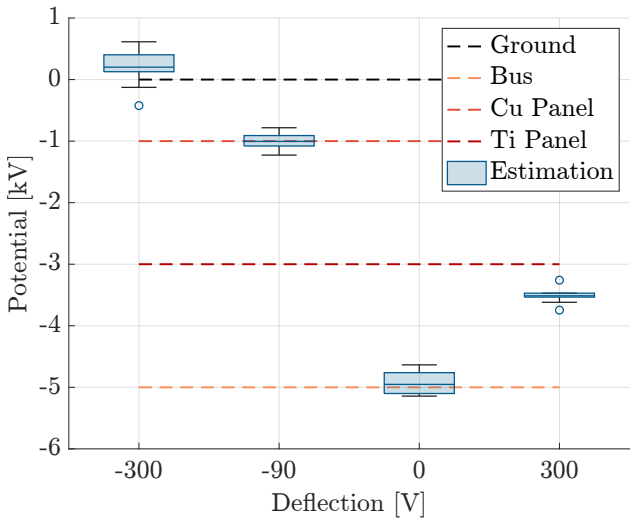

Fig. 5 Estimated potentials for different beam deflections

B. Simultaneous Estimation

If the electron beam impacts on multiple components that are charged to different potentials, then the total recorded x-ray spectrum is a superposition of the individual spectra from each component. This was investigated in Ref. 19 for a rotating target object. As the target rotates, the electron beam transitions from one component to another, and excites x-rays from multiple components. The x-ray detector records the spectrum for 20 seconds, while the target is rotating. As a result, the recorded spectrum includes information about the potential of both components. An approach was proposed in Ref. 19 to estimate multiple potentials from a single recorded x-ray spectrum. The potential of the first component is estimated from the total recorded spectrum using the linear curve fit as explained in Sec. II.A and applied in Sec. III.A. A theoretical spectrum is computed using the corresponding estimated landing energy and the theoretical x-ray models from Sec. II.B. This theoretical spectrum is subtracted from the total recorded spectrum to obtain a residual spectrum that corresponds to the individual spectrum of the second component. The potential of the second component is then estimated using the residual spectrum. Because the intensity of the theoretical spectrum is unknown, it is scaled to best fit the upper energy part of the recorded spectrum, for a 1.5 keV fitting window. This approach was tested in Ref. 19 for a rotating target object with two differentially charged components made of aluminum.

One of the limitations of the proposed approach is that the signal of some components may be significantly lower than that of other components, which makes the estimation of the potential less accurate. To investigate how many different potentials can be estimated from a single spectrum in a best-case-scenario, the spectra from the individual components used in Sec. III.A are manually super-imposed (without the spectrum from the chamber wall). This way, the signal from each component is similar in intensity. A sample super-imposed spectrum is shown in Fig. 6a, with the characteristic peaks for aluminum, titanium and copper visible. The highest (least negative) potential is estimated from this total spectrum, corresponding to the -1 kV of the copper panel. A theoretical spectrum for copper is generated and subtracted from the total spectrum, yielding the residual shown in Fig. 6b. The next potential is estimated the same way as the first one, but using the residual spectrum from the first estimation (Fig. 7a), corresponding to the -3 kV of the titanium panel. By subtracting the theoretical spectrum for titanium and for the given landing energy, another residual spectrum is obtained as shown in Fig. 7b and used to estimate the potential of the bus at -5 kV (Fig. 8a). The final residual spectrum in Fig. 8b is mostly noise.

Note that, even though the characteristic peaks are shown, the are identified using Matlab's `findpeaks()` function and removed for the estimation of the landing energy with the linear curve fit [12]. However, the presence of characteristic peaks in the upper energy part of the spectrum may still interfere with the estimation of the electric potential. First, removing the peaks essentially reduces the number of data points used for the linear fit. Linearly interpolating between the two endpoints of the removed characteristic peak is also disadvantageous because the least-squares solution would over-fit to the linearly interpolated part. Second, a characteristic peak in the upper end of the spectrum may also interfere with fitting the intensity of the theoretical spectrum, which in turn affects the estimated potential from the following residual spectrum. These challenges were not encountered in previous work on differential charging, because only

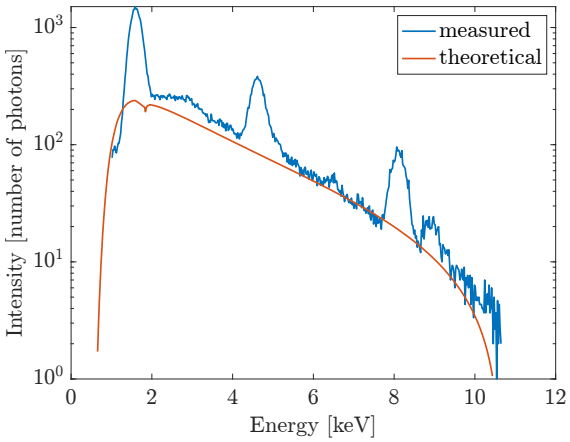

(a) original recorded spectrum

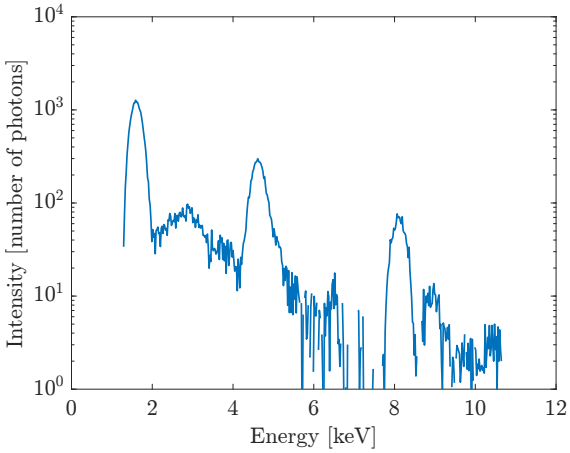

(b) first residual spectrum

Fig. 6 First estimation

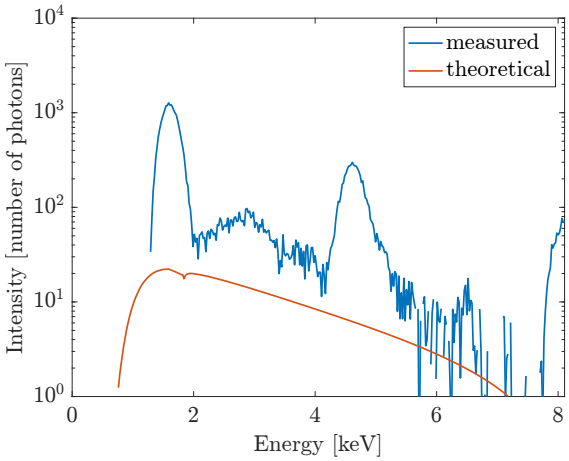

(a) residual spectrum from first estimation

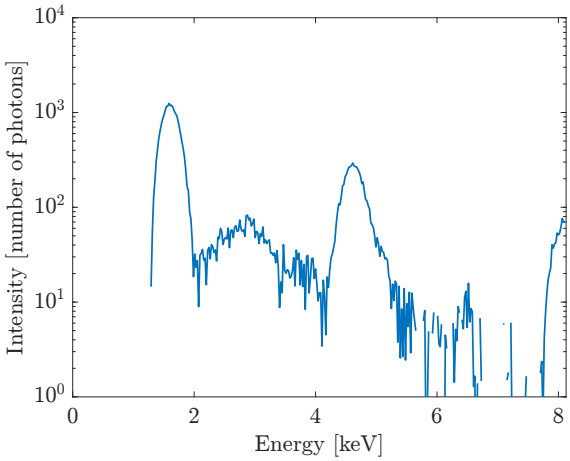

(b) second residual spectrum

Fig. 7 Second estimation

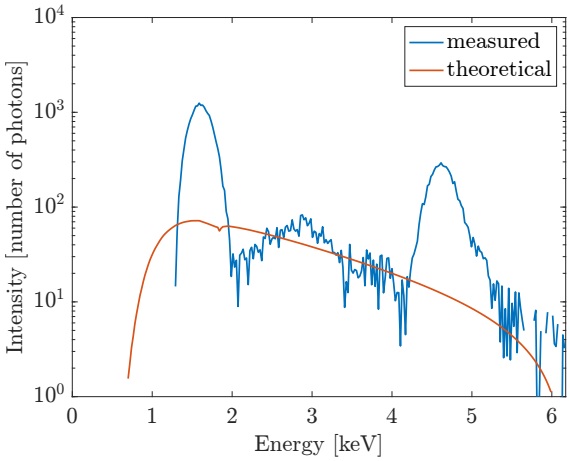

(a) residual spectrum from second estimation

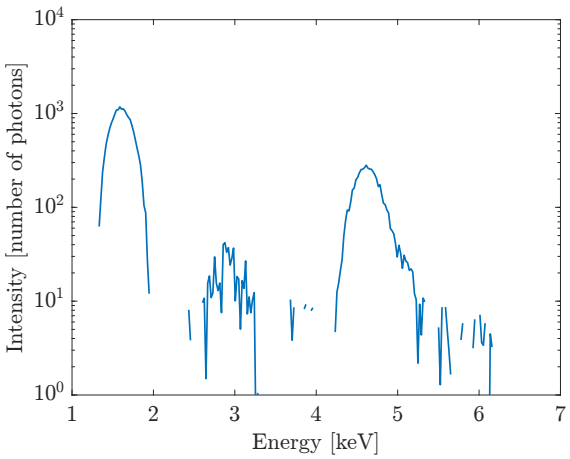

(b) third residual spectrum

Fig. 8 Third estimation

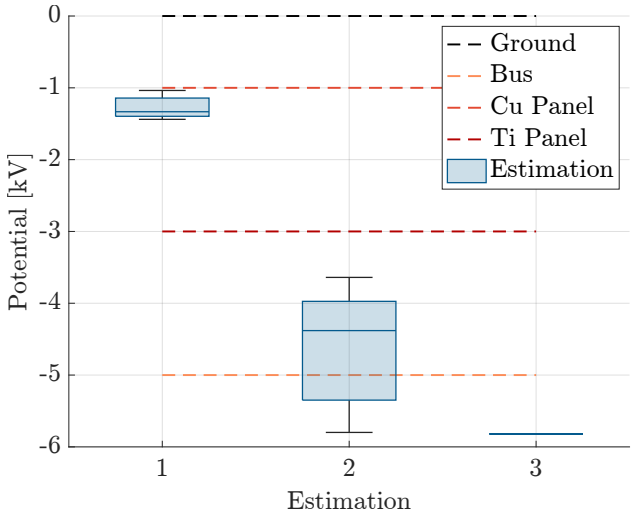

Fig. 9 Simultaneous estimation of potentials

aluminum components were used with a characteristic peak at 1.5 keV that is far away from the upper energy part of the spectrum.

Figure 9 shows a boxplot with the estimated potentials for each estimation step. Estimation 1 measures the highest potential, and each following estimation step measures the next lower potential. The errors of each estimation affect the next estimation, so the estimations become less accurate with every step. Additionally, a misfit of the intensity of the computed theoretical spectrum may decrease the intensity of the following residual spectrum, which also makes the next estimation less accurate.

IV. Conclusions

This paper experimentally investigates the estimation of electric potentials using x-rays. The target object used in the experiments consists of three components, each made of a different material and charged to a dissimilar potential. This enables investigating the effects of target material inhomogeneity and differential charging on the robustness of the x-ray based electric potential sensing method. Aluminum, titanium and copper components are used, resulting in characteristic x-ray peaks with energies between 1.5 and 8.9 keV in the recorded x-ray spectrum. The presence of characteristic peaks in the upper energy part of the x-ray spectrum provides some challenges for the potential estimation as they have to be filtered out from the recorded spectrum. This interferes with the linear least squares that is used for both the estimation of the electric potential and for the computation of the theoretical x-ray spectrum that is needed to estimate multiple potentials simultaneously from one recorded x-ray spectrum.

While the estimation of the first potential (the potential that is the least negative or most positive) is solely based on data from the recorded spectrum, the estimation of any additional potentials requires the computation of theoretical spectra. The dependence of the following estimations on the theoretical spectra also affects the accuracy of the estimations. Additionally, the errors of each estimation affect the next estimation, so as the errors pile up, the estimations become less accurate with every step. In conclusion, while the measurement of multiple potentials may be somewhat inaccurate in terms of the estimated potentials, the implemented method allows for the identification of differential charging on a target object.

Acknowledgments

This work was supported by the U.S. Air Force Office of Scientific Research under grant FA9550-20-1-0025. Julian Hammerl gratefully acknowledges funding from the NASA FINESST fellowship.

References

[1] Garrett, H. B., and Whittlesey, A. C., *Guide to Mitigating Spacecraft Charging Effects*, John Wiley & Sons, Inc., Hoboken, NJ, USA, 2012. https://doi.org/10.1002/9781118241400.

[2] Katz, I., Davis, V., and Snyder, D., "Mechanism for spacecraft charging initiated destruction of solar arrays in GEO," *36th AIAA Aerospace Sciences Meeting and Exhibit*, AIAA Paper 1998-1002, 1998, pp. 1–5. https://doi.org/10.2514/6.1998-1002.

[3] Brandhorst, H., and Rodiek, J., "Improving Space Utilization by Increasing Solar Array Reliability," *AIAA SPACE 2007 Conference and Exposition*, AIAA Paper 2007-6024, 2007, pp. 1–5. https://doi.org/10.2514/6.2007-6024.

[4] Wilson, K., and Schaub, H., "Impact of Electrostatic Perturbations on Proximity Operations in High Earth Orbits," *Journal of Spacecraft and Rockets*, Vol. 58, No. 5, 2021, pp. 1293–1302. https://doi.org/10.2514/1.A35039.

[5] Wilson, K., Romero-Calvo, Á., and Schaub, H., "Constrained Guidance for Spacecraft Proximity Operations Under Electrostatic Perturbations," *Journal of Spacecraft and Rockets*, 2022, pp. 1–13. https://doi.org/10.2514/1.A35162, in press.

[6] Schaub, H., and Moorer, D. F., "Geosynchronous Large Debris Reorbiter: Challenges and Prospects," *The Journal of the Astronautical Sciences*, Vol. 59, No. 1-2, 2012, pp. 161–176. https://doi.org/10.1007/s40295-013-0011-8.

[7] Hammerl, J., and Schaub, H., "Effects of Electric Potential Uncertainty on Electrostatic Tractor Relative Motion Control Equilibria," *Journal of Spacecraft and Rockets*, Vol. 59, No. 2, 2022, pp. 552–562. https://doi.org/10.2514/1.A35165.

[8] Bengtson, M., Hughes, J., and Schaub, H., "Prospects and Challenges for Touchless Sensing of Spacecraft Electrostatic Potential Using Electrons," *IEEE Transactions on Plasma Science*, Vol. 47, No. 8, 2019, pp. 3673–3681. https://doi.org/10.1109/TPS.2019.2912057.

[9] Wilson, K., and Schaub, H., "X-Ray Spectroscopy for Electrostatic Potential and Material Determination of Space Objects," *IEEE Transactions on Plasma Science*, Vol. 47, No. 8, 2019, pp. 3858–3866. https://doi.org/10.1109/TPS.2019.2910576.

[10] Wilson, K., Hammerl, J., and Schaub, H., "Using Plasma-Induced X-Ray Emission to Estimate Electrostatic Potentials on Nearby Space Objects," *Journal of Spacecraft and Rockets*, Vol. 59, No. 4, 2022, pp. 1402–1405. https://doi.org/10.2514/1.A35161.

[11] Wilson, K., Romero-Calvo, Á., Bengtson, M., Hammerl, J., Maxwell, J., and Schaub, H., "Development and characterization of the ECLIPS space environments simulation facility," *Acta Astronautica*, Vol. 194, 2022, pp. 48–58. https://doi.org/10.1016/j.actaastro.2021.12.037.

[12] Wilson, K. T., Bengtson, M. T., and Schaub, H., "X-ray Spectroscopic Determination of Electrostatic Potential and Material Composition for Spacecraft: Experimental Results," *Space Weather*, Vol. 18, No. 4, 2020, pp. 1–10. https://doi.org/10.1029/2019SW002342.

[13] Hammerl, J., Romero-Calvo, Á., López, A., and Schaub, H., "Touchless Potential Sensing of Complex Differentially-Charged Shapes Using X-Rays," *Proceedings of the AIAA SciTech 2022 Forum and Exposition*, 2022, pp. AIAA Paper 2022–2312. https://doi.org/10.2514/6.2022-2312.

[14] Hammerl, J., López, A., and Schaub, H., "Measuring Multiple Potentials of a Rotating and Differentially-Charged Object Simultaneously Using," *16th Spacecraft Charging Technology Conference*, 2022, pp. 1–6.

[15] Reimer, L., *Scanning Electron Microscopy*, 2nd ed., Springer Series in Optical Sciences, Springer, Berlin, Heidelberg, 1998. https://doi.org/10.1007/978-3-540-38967-5.

[16] Duane, W., and Hunt, F. L., "On X-Ray Wave-Lengths," *Phys. Rev.*, Vol. 6, No. 2, 1915, pp. 166–172. https://doi.org/10.1103/PhysRev.6.166.

[17] Brace, L. H., "Langmuir probe measurements in the ionosphere," *Geophysical Monograph-American Geophysical Union*, Vol. 102, 1998, pp. 23–36. https://doi.org/10.1029/GM102p0023.

[18] Lamoureux, M., and Charles, P., "General deconvolution of thin-target and thick-target Bremsstrahlung spectra to determine electron energy distributions," *Radiation Physics and Chemistry*, Vol. 75, No. 10, 2006, pp. 1220–1231. https://doi.org/10.1016/j.radphyschem.2006.06.006.

[19] Hammerl, J., López, A., Romero-Calvo, Á., and Schaub, H., "Touchless Potential Sensing of Differentially-Charged Spacecraft Using X-Rays," *Journal of Spacecraft and Rockets*, 2022, pp. 1–12. Accepted.

[20] McCall, G. H., "Calculation of X-ray bremsstrahlung and characteristic line emission produced by a Maxwellian electron distribution," *Journal of Physics D: Applied Physics*, Vol. 15, No. 5, 1982, pp. 823–831. https://doi.org/10.1088/0022-3727/15/5/012.

[21] Trincavelli, J., and Castellano, G., "The prediction of thick target electron bremsstrahlung spectra in the 0.25–50 keV energy range," *Spectrochimica Acta Part B: Atomic Spectroscopy*, Vol. 63, No. 1, 2008, pp. 1–8. https://doi.org/10.1016/j.sab.2007.11.009.

[22] An, Z., Tian, L., Zhu, J., and Liu, M., "Bremsstrahlung spectrum data for thick Al, Ti, Zr, Mo, and W targets by keV electron impact," *Data in Brief*, Vol. 17, 2018, pp. 744–746. https://doi.org/10.1016/j.dib.2018.01.111.

[23] Wilson, K., Romero-Calvo, Á., Bengtson, M., Hammerl, J., Maxwell, J., and Schaub, H., "Development and characterization of the ECLIPS space environments simulation facility," *Acta Astronautica*, Vol. 194, No. July 2021, 2022, pp. 48–58. https://doi.org/10.1016/j.actaastro.2021.12.037.

[24] Deslattes, R., Kessler Jr., E., Indelicato, P., de Billy, L., Lindroth, E., Anton, J., Coursey, J., Schwab, D., Chang, C., Sukumar, R., Olsen, K., and Dragoset, R., "X-ray Transition Energies," , 2005. URL https://dx.doi.org/10.18434/T4859Z.